Published by Institute of Physics Publishing for SISSA

Received: *August 24 , 2007*
Accepted: *October 18, 2007*
Published: *October 31, 2007*

Testing gluino spin with three-body decays

Csaba Csáki, Johannes Heinonen and Maxim Perelstein

Institute for High Energy Phenomenology,
Newman Laboratory of Elementary Particle Physics,
Cornell University, Ithaca, NY 14853, U.S.A.
E-mail: csaki@lepp.cornell.edu, heinonen@lepp.cornell.edu, maxim@lepp.cornell.edu

Abstract: We examine the possibility of distinguishing a supersymmetric gluino from a Kaluza-Klein gluon of universal extra dimensions (UED) at the Large Hadron Collider (LHC). We focus on the case when all kinematically allowed tree-level decays of this particle are 3-body decays into two jets and a massive daughter (typically weak gaugino or Kaluza-Klein weak gauge boson). We show that the shapes of the dijet invariant mass distributions differ significantly in the two models, as long as the mass of the decaying particle m_A is substantially larger than the mass of the massive daughter m_B. We present a simple analysis estimating the number of events needed to distinguish between the two models under idealized conditions. For example, for $m_A/m_B = 10$, we find the required number of events to be of order several thousand, which should be available at the LHC within a few years. This conclusion is confirmed by a parton level Monte Carlo study which includes the effects of experimental cuts and the combinatoric background.

Keywords: Large Extra Dimensions, Supersymmetry Phenomenology, Spin and Polarization Effects.

JHEP10(2007)107

Contents

JHEP10(2007)107

1. Introduction

Very soon, experiments at the Large Hadron Collider (LHC) will begin direct exploration of physics at the TeV scale. Strong theoretical arguments suggest that this physics will include new particles and forces not present in the Standard Model (SM). Several theoretically motivated extensions of the Standard Model at the TeV scale have been proposed. After new physics discovery at the LHC, the main task of the experiments will be to determine which of the proposed models, if any, is correct.

Unfortunately, there exists a broad and well-motivated class of SM extensions for which this task would be highly non-trivial. In these models, the new TeV-scale particles carry a new conserved quantum number, not carried by the SM states. The lightest of the new particles is therefore stable. Furthermore, the stable particle interacts weakly, providing a very attractive "weakly interacting massive particle" (WIMP) candidate for dark matter with relic abundance naturally in the observed range. Models of this class include the minimal supersymmetric standard model (MSSM) and a variety of other supersymmetric models with conserved R parity, Little Higgs models with T parity (LHT), and models with universal extra dimensions (UED) with Kaluza-Klein (KK) parity. All these models have a common signature at a hadron collider: pair-production of new states is followed by their prompt decay into visible SM states and the lightest new particle, which escapes the detector without interactions leading to a "missing transverse energy" signature. If this

universal signature is observed at the LHC, how does one determine which of these models is realized?

One crucial difference between the MSSM and models such as LHT or UED is the correlation between spins of the new particles and their gauge charges. In all these models, all (or many of) the new states at the TeV scale can be paired up with the known SM particles, with particles in the same pair carrying identical gauge charges. However, while in the LHT and UED models the two members of the pair have the same spin, in the MSSM and other supersymmetric models their spins differ by 1/2. Thus, measuring the spin of the observed new particles provides a way to discriminate among models.

Experimental determination of the spin of a heavy unstable particle with one or more invisible daughter(s) in hadron collider environment is a difficult task. One possibile approach, which recently received considerable attention in the literature [1 – 7], is to use angular correlations between the observable particles emitted in subsequent steps of a cascade decay, which are sensitive to intermediate particle spins. This strategy is promising, but its success depends on the availability of long cascade decay chains, which may or may not occur depending on the details of the new physics spectrum. It is worth thinking about other possible strategies for spin determination.

In this paper, we explore the possibility of using 3-body decays of heavy new particles to determine their spin. The most interesting example is the 3-body decay of the MSSM gluino into a quark-antiquark pair and a weak gaugino,

$$\tilde{g} \to q + \bar{q} + \chi. \tag{1.1}$$

In a large part of the MSSM parameter space, this decay has a large branching ratio: this occurs whenever all squarks are heavier than the gluino. Under the same condition, gluino pair-production dominates the SUSY signal at the LHC. The main competing gluino decay channel in this parameter region is a two-body decay $\tilde{g} \to g\chi$, which first arises at one-loop level and generically has a partial width comparable to the tree-level decay (1.1). The gluino decay patterns in this parameter region have been analyzed in detail in ref. [8]. We will argue that the invariant mass distribution of the jets produced in reaction (1.1) contains non-trivial information about the gluino spin, and can be used to distinguish this process from, for example, its UED counterpart, $g^1 \to q + \bar{q} + B^1/W^1$.

It is important to note that the jet invariant mass distribution we study depends not just on the spin of the decaying particle, but also on the helicity structure of the couplings which appear in the decay (1.1), as well as on the masses of the decaying particle, the invisible daughter, and the off-shell particles mediating the decay. If all these parameters were measured independently, the jet invariant mass distribution would unambiguously determine the spin. However, independent determination of many of the relevant parameters will be very difficult or impossible at the LHC. In this situation, proving the spin-1/2 nature of the decaying particle requires demonstrating that the experimentally observed curve cannot be fitted with any of the curves predicted by models with other spin assignments, independently of the values of the unknown parameters. This considerably complicates our task. Still, interesting information can be extraced. For example, we will show that, even if complete ignorance of the decaying and intermediate particle masses is assumed, the jet

JHEP10(2007)107

invariant mass distribution allows one to distinguish between the decay (1.1) in the MSSM and its UED counterpart (assuming the couplings specified by each model) at the LHC.

The paper is organized as follows. After setting up our notation and reviewing the basics of three-body kinematics in section 2, we present a simple toy model showing how dijet invariant mass distributions from three-body decays can be used to probe the nature of the decaying particle and its couplings in section 3. Section 4 discusses using this observable for MSSM/UED discrimination, and contains the main results of the paper. Section 5 contains the conclusions. Appendix A contains the polarization analysis of the decay $g^1 \to q + \bar{q} + B^1/W^1$ in UED, which sheds some light on the main features of the dijet invariant mass distribution in this case. Appendix B contains a brief review of the Kullback-Leibler distance, a statistical measure used in our analysis.

2. The setup and kinematics

We are interested in three-body decays of the type

$$A \to q + \bar{q} + B, \tag{2.1}$$

where A and B are TeV-scale particles. The main focus of this paper will be on the case when A is the gluino of the MSSM or the KK gluon of the UED model, and B is a neutalino or chargino of the MSSM or a KK electroweak gauge boson of the UED; however the discussion in this section applies more generally. We assume that q and $\bar{q}$ are massless, and denote their four-momenta by p_1 and p_2 respectively. To describe the kinematics in Lorentz-invariant terms, we introduce the "Mandelstam variables",

$$\begin{aligned} m_{12}^2 &\equiv s = (p_1 + p_2)^2 = (p_A - p_B)^2 \,, \\ m_{1B}^2 &\equiv u = (p_1 + p_B)^2 = (p_A - p_2)^2 \,, \\ m_{2B}^2 &\equiv t = (p_2 + p_B)^2 = (p_A - p_1)^2 \,, \end{aligned} \tag{2.2}$$

of which only two are independent since

$$s + t + u = m_A^2 + m_B^2. \tag{2.3}$$

The allowed ranges for the Mandelstam variables are determined by energy and momentum conservation; in particular,

$$0 \le s \le s^{\max} \equiv (m_A - m_B)^2. \tag{2.4}$$

We will assume that p_B cannot be reconstructed, either because B is unobservable or is unstable with all decays containing unobservable daughters. Moreover, since the parton center-of-mass frame is unknown, no information is available about the motion of particle A in the lab frame. Due to these limitations, the analysis should use observables that can be reconstructed purely by measuring the jet four-momenta, and are independent of the velocity of A in the lab frame. The only such observable is s, and the object of interest to us is the distribution $d\Gamma/ds$. This is given by

$$\frac{d\Gamma}{ds} = \frac{1}{64\pi^3} \frac{s}{m_A^2} \int_{E_B - p_B}^{E_B + p_B} \frac{dy}{(m_A - y)^2} \, |\bar{\mathcal{M}}|^2 \,, \tag{2.5}$$

where

$$E_B = \frac{m_A^2 + m_B^2 - s}{2m_A},$$
$$p_B = \sqrt{E_B^2 - m_B^2}, \tag{2.6}$$

and $\mathcal{M}$ is the invariant matrix element for the decay (2.1), with the bar denoting the usual summation over the final state spins and other quantum numbers and averaging over the polarization and other quantum numbers of A. This procedure should take into account the polarization of A, if it is produced in a polarized state. In the examples of this paper, production is dominated by strong interactions and A will always be produced unpolarized. For a more detailed discussion of polarized decays see appendix A.

The quantity $|\bar{\mathcal{M}}|^2$ can be expressed in terms of the variables (2.2); substitutions

$$t \to m_A^2 - \frac{s m_A}{m_A - y}, \quad u \to \frac{sy}{m_A - y} + m_B^2 \tag{2.7}$$

should be made in $|\bar{\mathcal{M}}|^2$ before performing the integral in eq. (2.5). Notice that eq. (2.5) is valid in the rest frame of the particle A; however, since s is Lorentz-invariant, its Lorentz transformation is a trivial overall rescaling by time dilation, and the shape of the distribution is unaffected. The strategy we will pursue is to use this shape to extract information about the decay matrix element $\mathcal{M}$, which is in turn determined by the spins and couplings of the particles A and B.

To separate the effects of non-trivial structure of the decay matrix element from those due merely to kinematics, it will be useful to compare the dijet invariant mass distributions predicted by various theories to the "pure phase space" distribution, obtained by setting the matrix element to a constant value. From eq. (2.5), the phase space distribution is given by

$$\frac{d\Gamma}{ds} = \frac{1}{32\pi^3} \frac{|\mathbf{p}_B|}{m_A} \propto \sqrt{(s - m_A^2 - m_B^2)^2 - 4m_A^2 m_B^2}. \tag{2.8}$$

This distribution[1] is shown by a solid black line in figure 1. Notice that the phase space distribution has an endpoint at $s = s^{\max}$, with the asymptotic behavior given by

$$\frac{d\Gamma}{ds} \sim (s - s^{\max})^{1/2} \tag{2.9}$$

as the endpoint is approached.

3. Chiral structure in three-body decays: a toy model

To illustrate how the chiral structure of the couplings involved in the decay (2.1) can be determined from the dijet invariant mass distribution, consider a situation when the

[1]Since we are concerned with the shapes of the dijet invariant mass distributions in various models and not their overall normalizations, all distributions appearing on the plots throughout this paper are normalized to have the same partial width $\Gamma = \int_0^{s^{\max}} \frac{d\Gamma}{ds}\, ds$.

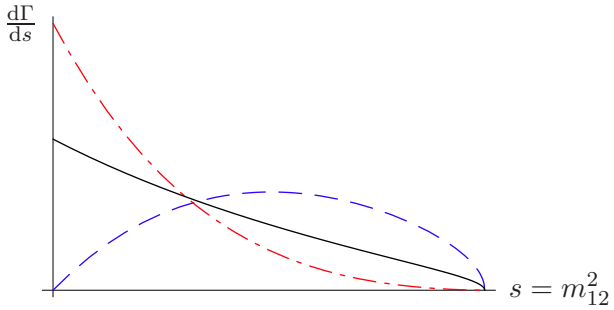

Figure 1: Dijet invariant mass distribution for the toy model 1 (blue/dashed) and model 2 (red/dot-dashed) compared to phase space (black/solid) for $M_*/m_A = 1.5$ and $m_B/m_A = 0.1$.

particles A and B are real scalars. Introduce a massive Dirac fermion Ψ of mass $M_* > m_A$, and consider the following two models: model 1 defined by

$$\mathcal{L}_1 \;=\; y_A A\bar{\Psi}P_L q + y_B B\bar{\Psi}P_R q + \text{h.c.} \tag{3.1}$$

and model 2 defined by

$$\mathcal{L}_2 \;=\; y_A A\bar{\Psi}P_L q + y_B B\bar{\Psi}P_L q + \text{h.c.} \tag{3.2}$$

The matrix element for the decay (2.1) in model 1 is given by

$$\sum_{\text{spin}} |\mathcal{M}_1|^2 \;=\; 2y_A^2 y_B^2 (M_*^2\, s)\left(\frac{1}{(t-M_*^2)^2} + \frac{1}{(u-M_*^2)^2}\right), \tag{3.3}$$

while in model 2 it is given by

$$\sum_{\text{spin}} |\mathcal{M}_2|^2 \;=\; 2y_A^2 y_B^2 \left((m_A^2 + m_B^2)tu - m_A^2 m_B^2\right)\left(\frac{1}{t-M_*^2} + \frac{1}{u-M_*^2}\right)^2. \tag{3.4}$$

The dijet invariant mass distributions in the two models are shown by the blue/dashed line (model 1) and red/dot-dashed line (model 2) in figure 1. Their strikingly different shapes are due to the angular momentum conservation law and to the different helicity structure of the couplings. To understand this, consider this decay in the A rest frame. In this frame, $s = 2E_1E_2(1-\cos\theta_{12})$. When $s = 0$, the quark and the antiquark travel in the same direction, as illustrated in figure 2. Since A and B have zero spin, the sum of the quark and antiquark helicities must vanish for this kinematics. In model 1, the quark and the antiquark have the same helicity, and the decay is forbidden for $s = 0$; in model 2, it is allowed. In contrast, when $s = s^{\max}$, the particle B is at rest, and the quark and the antiquark travel in the opposite directions. By angular momentum conservation, their helicities must be equal. In model 1, this is the case, and the distribution approaches that of pure phase space in the limit $s \to s^{\max}$. In model 2, this kinematics is forbidden, the matrix element vanishes at the endpoint, and the distribution behaves as $d\Gamma/ds \propto (s - s^{\max})^{3/2}$.

JHEP10(2007)107

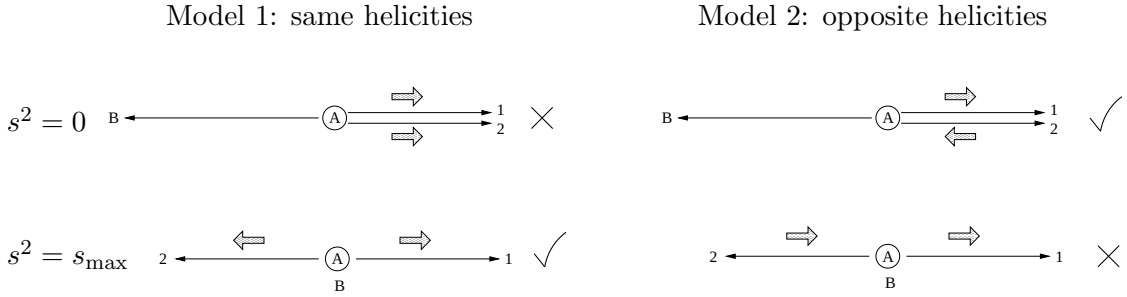

Figure 2: Momenta (long arrows) and helicities (short arrows) in the A rest frame for $s = m_{12}^2 = 0$ and $s = m_{12}^2 = s^{\max}$ in the two toy models of section 3.

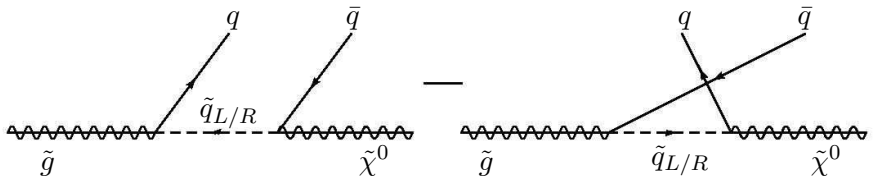

Figure 3: The Feynman diagrams for gluino three-body decay in the MSSM. Note that the crossing of the quarks results in a relative minus sign.

4. Model discrimination: SUSY versus UED

In this section, we will show that measuring the shape of the dijet invariant mass distribution arising from a three-body decay of a heavy colored particle may allow to determine whether the decaying particle is the gluino of the MSSM or the KK gluon of the UED model. We will begin by comparing the analytic predictions for the shapes of the two distributions at leading order. We will then present a parton-level Monte Carlo study which demonstrates that the discriminating power of this analysis persists after the main experimental complications (such as the combinatioric background, finite energy resolution of the detector, and cuts imposed to suppress SM backgrounds) are taken into account.

4.1 Gluino decay in the MSSM

We consider the MSSM in the region of the parameter space where all squarks are heavier than the gluino, forbidding the two-body decays $\tilde{g} \to \tilde{q}q$. In this situation, gluino decays through three-body channels. We study the channel

$$\tilde{g}(p_A) \to q(p_1) + \bar{q}(p_2) + \tilde{\chi}_1^0(p_B), \tag{4.1}$$

where q and $\bar{q}$ are light (1st and 2nd generation) quarks, and $\tilde{\chi}_1^0$ is the lightest neutralino which we assume to be the LSP. (Note that many of our results would continue to hold if $\tilde{\chi}_1^0$ is replaced with a heavier neutralino or a chargino. The only extra complication in these cases would be a possible additional contribution to the combinatoric background from the subsequent cascade decay of these particles.) The leading-order Feynman diagrams for the process (4.1) are shown in figure 3; the vertices entering these diagrams are well known (see for example ref. [9]). The spin-summed and averaged matrix element-squared has the

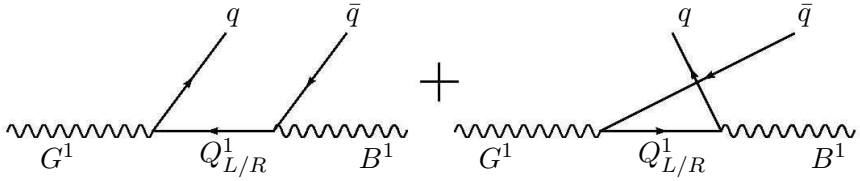

Figure 4: The Feynman diagrams for the KK gluon three-body decay in UED. Unlike in the MSSM case, there is no relative minus sign, since what looks like a crossing of the quarks, is actually equivalent to a crossing of the gauge bosons.

form (up to an overall normalization constant)

$$\sum_{\text{spin}} |\mathcal{M}_{\text{MSSM}}|^2 \;=\; |C_L|^2 F(s,t,u;M_{L*}) + |C_R|^2 F(s,t,u;M_{R*})\,, \tag{4.2}$$

where

$$F(s,t,u;M) = \frac{(m_A^2-t)(t-m_B^2)}{(t-M^2)^2} + \frac{(m_A^2-u)(u-m_B^2)}{(u-M^2)^2} + 2\frac{m_A m_B s}{(u-M^2)(t-M^2)}\,. \tag{4.3}$$

Here m_A, m_B, M_{L*} and M_{R*} are the masses of the gluino, the neutralino, the squarks $\tilde{q}_L$ and $\tilde{q}_R$, respectively. In order to keep the analysis general, we will not assume any relationships (such as mSUGRA contraints) among these parameters, and will always work in terms of weak-scale masses. We also define

$$\begin{aligned} C_L &= T_q^3 N_{12} - t_w (T_q^3 - Q_q) N_{11}\,, \\ C_R &= t_w Q_q N_{11}\,, \end{aligned} \tag{4.4}$$

where $T_u^3 = +1/2, T_d^3 = -1/2, Q_u = +2/3, Q_d = -1/3, t_w = \tan\theta_w$, and N is the neutralino mixing matrix[2] in the basis $(\tilde{B}, \tilde{W}^3, \tilde{H}_u^0, \tilde{H}_d^0)$. We have neglected the mixing between the left-handed and right-handed squarks, which is expected to be small in the MSSM. Large mixing in the stop sector may be present, and is actually preferred by fine-tuning arguments in the MSSM (see, e.g., ref. [10]). However, events with top quarks in the final state are characterized by more complicated topologies and can be experimentally distinguished from the events with light quarks that we are focussing on here. Since light up and down type quarks are experimentally indistinguishable, the dijet invariant mass distribution $d\Gamma/ds$ should include both the contributions of up-type and down-type squarks.

4.2 Decay of the gluon KK mode in the UED model

The counterpart of the decay (4.1) in the universal extra dimensions (UED) model is the decay

$$g^1(p_A) \to q(p_1) + \bar{q}(p_2) + B^1(p_B), \tag{4.5}$$

where g^1 and B^1 are the first-level Kaluza-Klein (KK) excitations of the gluon and the hypercharge gauge boson, respectively. We ignore the mixing between B^1 and the KK

[2]We assume that N is real. It is always possible to redefine the neutralino fields to achieve this. However one should keep in mind that the neutralino eigenmasses may be negative with this choice.

mode of the W^3 field, which is small provided that the radius of the extra dimension is small, $R \ll 1/M_W$, and assume that the B^1 is the LTP. As in the MSSM case, the decay (4.5) is expected to have a substantial branching fraction when all KK quarks Q_R^1 and Q_L^1 are heavier than the KK gluon. Note that in the original UED model [11], the KK modes of all SM states were predicted to be closely degenerate in mass around $M = 1/R$; it was however later understood [12] that kinetic terms localized on the boundaries of the extra dimension can produce large mass splittings in the KK spectrum. Since such kinetic terms are consistent with all symmetries of the theory, we will assume that they are indeed present, and treat the masses of the g^1, B^1, Q_R^1 and Q_L^1 fields as free parameters.

The leading-order Feynman diagrams for the decay (4.5) are shown in figure 4. (We ignored the contribution of the diagrams mediated by $Q_{L/R}^i$ with $i \geq 2$, which are suppressed by the larger masses of the higher KK modes.) The relevant couplings have the form

$$\begin{aligned} &g_3 G_\mu^1 \left[\bar{q}\gamma^\mu P_R Q_R^1 + \bar{q}\gamma^\mu P_L Q_L^1 + \bar{Q}_R^1 \gamma^\mu P_R q + \bar{Q}_L^1 \gamma^\mu P_L q\right] + \\ &g_1 B_\mu^1 \left[Y(q_R)\,\bar{q}\gamma^\mu P_R Q_R^1 + Y(q_L)\,\bar{q}\gamma^\mu P_L Q_L^1 + Y(q_R)\,\bar{Q}_R^1 \gamma^\mu P_R q + Y(q_L)\,\bar{Q}_L^1 \gamma^\mu P_L q\right], \end{aligned} \tag{4.6}$$

where $Y(q_L) = 1/6, Y(u_R) = +2/3$ and $Y(d_R) = -1/3$ are the hypercharges. The structure of the couplings between the KK gauge bosons and SM (or KK) quarks are unaffected by brane-localized kinetic terms as long as these terms are flavor-independent.

The spin-summed and averaged matrix element-squared has the form (up to an overall normalization constant)

$$\sum_{\text{spin}} |\mathcal{M}_{\text{UED}}|^2 \;=\; Y_L^2\, G(s,t,u;M_{L*}) + Y_R^2\, G(s,t,u;M_{R*})\,, \tag{4.7}$$

where M_{L*} and M_{R*} are the masses of the left- and right-handed quark KK modes Q_L^1 and Q_R^1, and

$$G(s,t,u;M) = \frac{h_1(s,t,u)}{(t-M^2)^2} + \frac{h_1(s,u,t)}{(u-M^2)^2} + 2\frac{h_2(s,t,u)}{(t-M^2)(u-M^2)}, \tag{4.8}$$

with

$$\begin{aligned} h_1(s,t,u) &= 4(tu - m_A^2 m_B^2) + \frac{t^2}{m_A^2 m_B^2}\left(2s(m_A^2+m_B^2) + tu - m_A^2 m_B^2\right)\,, \\ h_2(s,t,u) &= 4s(m_A^2+m_B^2) - \frac{tu}{m_A^2 m_B^2}\left(2s(m_A^2+m_B^2) + tu - m_A^2 m_B^2\right)\,. \end{aligned} \tag{4.9}$$

4.3 Model discrimination: a simplified analysis

Armed with the expressions (4.2) and (4.7), it is straightforward to obtain the dijet invariant mass distributions for gluino and KK gluon decays and compare them. For example, the two distributions for a particular choice of parameters, along with the pure phase space distribution, are shown in figure 5. While not as strikingly different as the two toy models of section 3, the curves predicted by the MSSM and the UED are clearly distinct. (The suppression of the UED distribution compared to phase space around $s = 0$ and $s = s_{\max}$ can be easily understood using angular momentum conservation, as explained in

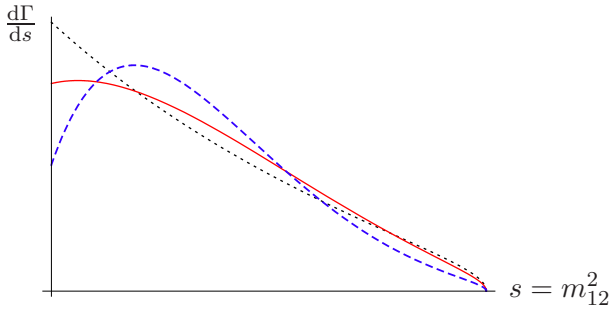

Figure 5: Dijet invariant mass distribution for the UED (blue/dashed) and the MSSM (red/solid) models, compared to pure phase space (black/dotted) for $M_{L*}/m_A = M_{R*}/m_A = 1.5$ and $m_B/m_A = 0.1$.

appendix A.) In this section, we will perform a simplified analysis of the discriminating power of these distributions, ignoring experimental complications such as cuts, finite energy resolution, combinatoric and SM backgrounds, and systematic errors. We will return to include some of these complications in the following section.

The distrubution in each model depends on a number of parameters, including the mass of the mother particle m_A, the mass of the invisible daughter m_B, and the masses of intermediate particles: $(\tilde{u}_L, \tilde{d}_L, \tilde{u}_R, \tilde{d}_R)$ in the MSSM case and $(U_L^1, D_L^1, U_R^1, D_R^1)$ in the UED case. We assume that the partners of the up-type quarks of the first two generations and the down-type quarks for all three generations are degenerate, and do not include the diagrams with intermediate stops (or KK tops) since they produce tops in the final state. Furthermore, since the Yukawa couplings for the first two generations are small, it is safe to assume that $m(\tilde{u}_L) = m(\tilde{d}_L)$ in the MSSM and $m(U_L^1) = m(D_L^1)$ in UED. Since an overall rescaling of all masses does not affect the shape of the distribution, we need four dimensionless parameters to specify the mass spectrum in each model; we use the particle masses in units of m_A. Experimentally, these four parameters may be very difficult to obtain independently. A direct measurement of the masses of squarks/KK quarks may well be impossible, since these particles may be too heavy to be produced on-shell. Also, while it is easy to measure $m_A - m_B$ (one can use the endpoint of the dijet invariant mass distribution or other simple observables such as the effective mass [13] or its variations [14]), it is much more difficult to measure m_A and m_B individually [15], which would be required in order to obtain m_B/m_A. In this study, we will conservatively assume no prior knowledge of any of these parameters. (Of course, if some independent information about them is available, for example the overall mass scale is constrained by production cross section considerations, this information can be folded into our analysis, increasing its discriminating power.) In addition to the unknown masses, the matrix elements in the MSSM depend on the neutralino mixing matrix elements, N_{11} and N_{12}, although only the ratio N_{11}/N_{12} affects the shape of the distribution. Again, this parameter is difficult to measure at the LHC, and we will assume that it is unknown; fortunately, the effect of varying it is quite small.

To quantify the discriminating power of the proposed observable, we use the following

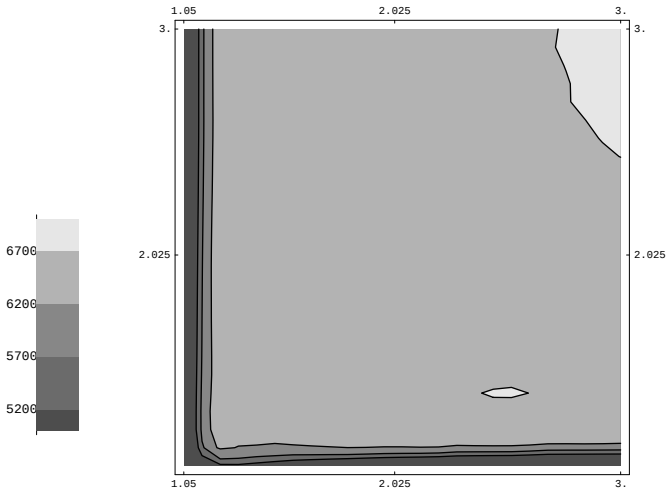

Figure 6: Number of events required to distinguish the MSSM and the UED models based on the invariant mass distributions of jets from three-body $\tilde{g}/G^1$ decays.

procedure. We assume that the experimental data is described by the MSSM curve with a particular set of parameters. We then ask, how many events (assuming statistical errors only) would be required to rule out the UED as an explanation of this distribution? To answer this question, we scan over 50000 points in the UED parameter space:

$$\begin{aligned} m_B/m_A &= (0 \ldots 0.5), \quad M(Q_L^1)/m_A = (1.05 \ldots 3.0), \\ M(D_R^1)/m_A &= (1.05 \ldots 3.0), \quad M(U_R^1)/m_A = (1.05 \ldots 3.0). \end{aligned} \tag{4.10}$$

For each point in the scan, we compute the Kullback-Leibler (KL) distance (see appendix B) between the UED distribution with the parameters at that point, and the "experimental" distribution. We then find the "best-fit UED" point, which is the point that gives the smallest KL distance among the scanned sample. Finally, we compute the number of events required to rule out the best-fit UED point at a desired confidence level.

The results of this analysis are shown in figure 6. The MSSM parameters used to generate the "data" are: $m_B = 0.1 m_A$, $m(\tilde{u}_R) = m(\tilde{d}_R) \equiv m_R, m(\tilde{u}_L) = m(\tilde{d}_L) \equiv m_L$, $N_{11}/N_{12} = 1$. The parameters m_L and m_R were then scanned between $1.05 m_A$ and $3 m_A$, and for each point in the scan the procedure described in the previous paragraph was performed. Figure 6 shows the number of events required to rule out the UED interpretation of the signal at the 99.9% c.l. (In the language of appendix B, this corresponds to $R = 1000$.) In a typical point in the model parameter space, about 6000 events are required. For comparison, the pair-production cross section for a 1 TeV gluino at the LHC is about 600 fb, corresponding to 12000 gluinos/year at the initial design luminosity of $10\,\mathrm{fb}^{-1}$/year. The number of events useful for the measurement studied here depends on the branching ratio of the decay (1.1). Since this branching ratio is generically of order one, we expect $O(10^3)$ useful events/year at the initial stages of the LHC running. Thus, at least under the highly idealized conditions of this simplified analysis, this method of model discrimination is quite promising in a wide range of reasonable model parameters.

JHEP10(2007)107

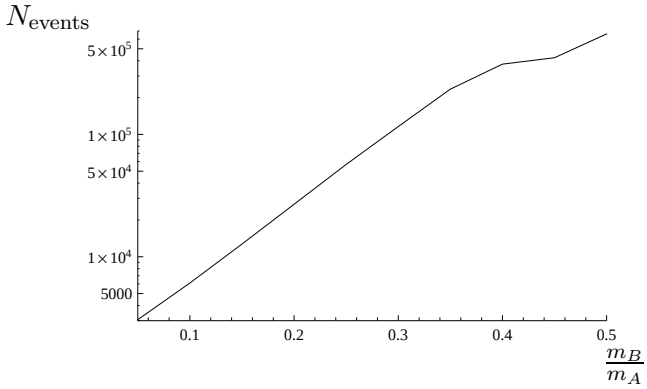

Figure 7: Number of events required to distinguish the MSSM and the UED models, as a function of m_B/m_A of the "true" model.

We checked that the conclusions of this analysis are approximately independent of the value of N_{11}/N_{12} used to generate the "data". They do, however, depend sensitively on the ratio m_B/m_A: as m_B/m_A grows, the MSSM and UED distributions become more and more alike. This is illustrated in figure 7, which shows the number of events needed to rule out the "wrong" model (assumed to be UED) at the 99.9% c.l., as a function of m_B/m_A of the "true" model (assumed to be the MSSM with $m(\tilde{u}_R) = m(\tilde{d}_R) = m(\tilde{u}_L) = m(\tilde{d}_L) = 1.5m_A$ and $N_{11}/N_{12} = 1$). The UED scan parameters are the same as in eq. (4.10), except that we vary $m_B/m_A = (0 \ldots 0.9)$ in this case. It is clear that the discriminating power of the dijet invariant mass distribution falls rapidly (approximately exponentially) with growing m_B/m_A. This can be understood as follows. The main feature of the invariant mass distributions that allows for model discrimination is the presence of the sharp dip at $s = 0$ in the UED case. According to the Goldstone boson equivalence theorem, if the daughter particle B in the UED case is highly boosted, the decays into its longitudinal component will dominate. The particle B is highly boosted in the vicintiy of $s = 0$, provided that the mass ratio m_B/m_A is small; as m_B/m_A grows, the boost becomes less pronounced and the decays into the longitudinal component of B are less dominant. This is illustrated in figure 8, which compares the ratio of partial decay rates into the longitudinal and transverse modes of B for $m_B/m_A = 0.1$ and $m_B/m_A = 0.5$. However, it is exactly the decays into the longitudinal mode of B that are mainly responsible for the characteristic dip at $s = 0$; this feature is far less pronounced for the decays into transverse modes. This means that as m_B/m_A is increased, the dip gradually disappears, and the discriminating power of our observable fades away.

We have also checked that the results of our analysis are approximately independent of which model, MSSM or UED, is assumed to be the "true" one giving the experimental data. For this one has to assume that the mass spectrum of the UED model is adjusted to match the MSSM spectrum, which can be achieved by adding large brane-localized kinetic terms for the gluons and quarks.

4.4 Model discrimination: a test-case Monte Carlo study

Given the large number of simplifying assumptions made in the analysis of the previous

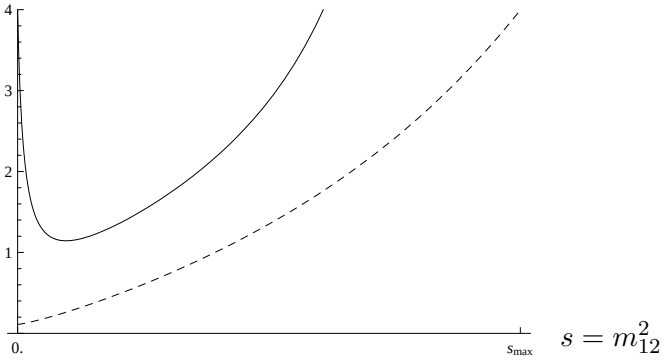

Figure 8: Ratio of the decay distributions of A into the longitudinal component of B to the decay distributions into the transverse components of B for $m_B/m_A = 0.1$(solid) and $m_B/m_A = 0.5$(dashed). For low m_B/m_A the daughter particle is highly boosted at $s = 0$ and will mainly be longitudinally polarized. As m_B increases, the transeverse polarization becomes more important.

section, a skeptical reader may well wonder how meaningful the results presented above are. In this section, we will repeat the analysis in a more realistic setting: effects of experimental cuts and combinatoric background will be included. We will also bin the distributions, to approximate the effects of finite jet energy resolution. Since this analysis involves generating large samples of Monte Carlo (MC) events for each model, we were not able to perform a scan over the model parameter space, as we did in the previous section. Instead, we will present a test case, comparing the MSSM distribution for a single point in the MSSM parameter space with the distribution generated by the "best-fit" UED model for that point.

The chosen MSSM point has the following parameters: $m_A = 1\,\text{TeV}$, $m_B = 0.1 m_A = 100\,\text{GeV}$, $M(\tilde{Q}_L) = M(\tilde{u}_R) = M(\tilde{d}_R) = 1.5\,\text{TeV}$. The corresponding "best-fit" UED point, found by the procedure described in the previous section, has the following parameters: $m_A = 1.06\,\text{TeV}$, $m_B = 0.15 m_A = 160\,\text{GeV}$, $M(Q_L^1) = M(u_R^1) = M(d_R^1) = 1.6\,\text{TeV}$. (Note that the value of $m_A - m_B$, which can be determined independently, is the same for these two points.) Using `MadGraph/MadEvent v4.1` [16] event generator, we have simulated a statistically significant sample (about 20000) of parton-level Monte Carlo events for each model in pp collisions at $\sqrt{s} = 14\,\text{TeV}$. The simulated processes are

$$pp \to qq\bar{q}\bar{q}\chi_1^0\chi_1^0 \tag{4.11}$$

in the MSSM, and its counterpart,

$$pp \to qq\bar{q}\bar{q}B^1B^1, \tag{4.12}$$

in UED. With the chosen model parameters, the dominant contribution to the processes (4.11) and (4.12) comes from pair-production of $\tilde{g}/G^1$, followed by the three-body decay (1.1), which is of primary interest to us. In the MC simulation, we did not demand that the $\tilde{g}/G^1$ be on-shell; the full tree-level matrix elements for the $2 \to 6$ reactions (4.11) and (4.12) were simulated, so that the subdominant contributions with off-shell $\tilde{g}/G^1$ are

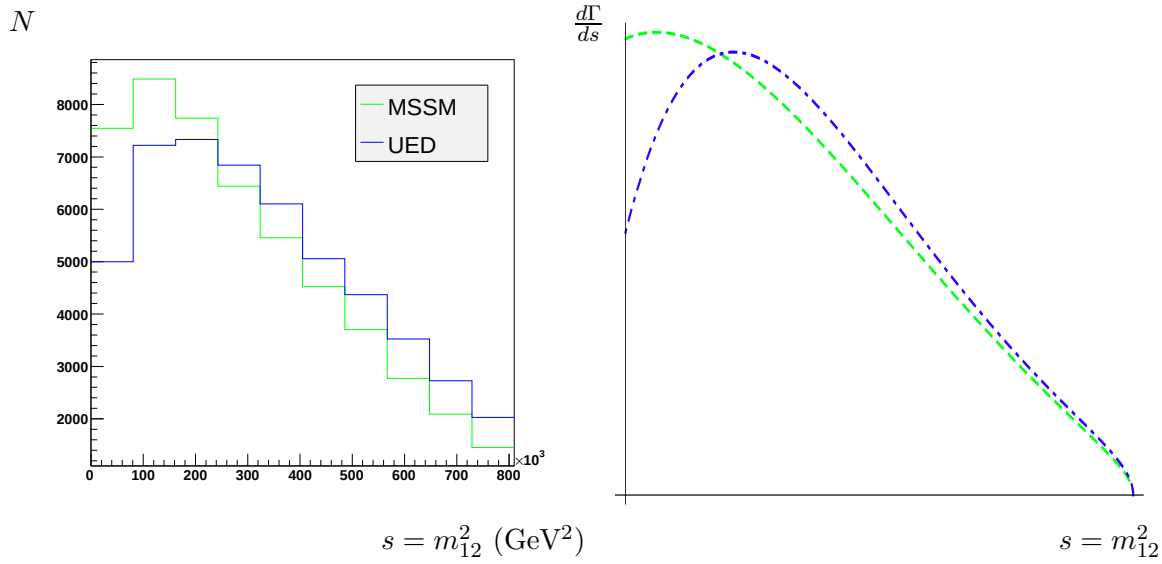

Figure 9: Left panel: Dijet invariant mass distributions from the MSSM reaction $pp \to qq\bar{q}\bar{q}\chi_1^0\chi_1^0$ (green/light-gray), and its UED counterpart $pp \to qq\bar{q}\bar{q}B^1B^1$ (blue/dark-gray), including realistic experimental cuts and the combinatoric background (Monte Carlo simulation). Right panel: Theoretical dijet invariant mass distributions from a single gluino/KK gluon decay with the same model parameters and no experimental cuts.

included. We imposed the following set of cuts on the generated events:

$$\eta_i \leq 4.0; \quad \Delta R(i,j) \geq 0.4; \quad p_{T,i} \geq 100 \text{ GeV}; \quad \not{E}_T \geq 100 \text{ GeV}, \tag{4.13}$$

where $i = 1 \ldots 4$, $j = i + 1 \ldots 4$ label the four (anti)quarks in each event. The first three cuts are standard for all LHC analyses, reflecting the finite detector coverage, separation required to define jets, and the need to suppress the large QCD background of soft jets. The $\not{E}_T$ cut is common to all searches for models where new physics events are characterized by large missing transverse energy, such as the MSSM and UED models under consideration. Detailed studies have shown that this cut is quite effective in suppressing the SM backgrounds, including both the physical background, $4j + Z$, $Z \to \nu\bar{\nu}$, and a variety of instrumental backgrounds (see, for example, the CMS study [17]). While we have not performed an independent analysis of the SM backgrounds, based on previous work we expect that, with a sufficiently restrictive $\not{E}_T$ cut, one will be able to obtain a large sample of new physics events with no significant SM contamination.

The dijet invariant mass distruibutions obtained from the MSSM and UED MC samples are shown in figure 9. The distributions are normalized to have the same total number of events, since the overall normalization is subject to large systematic uncertainties and we do not use any normalization information in our study. Note that for each MC event, we include all 6 possible jet pairings; 4 out of these correspond to combining jets that do *not* come from the same decay, and thus do not follow the theoretical distributions computed above. In figure 9, we selected the jet pairs with $s \leq (m_A - m_B)^2$. This selection can be implemented in a realistic experimental situation because $m_A - m_B$ can be measured independently. All pairs with larger values of s arise from the wrong jet

pairings. However, some of the wrong jet pairs do have s in the selected range, forming a combinatoric background to the distribution we want to study. Nevertheless, it is clear from figure 9 that even after realistic cuts (4.13) and the combinatoric background are included, the distributions in the two models retain their essential shape difference expected from the simplified theoretical analysis of the previous section. Assuming that the experimental data is described by the MSSM histogram and ignoring systematic uncertainties, we find (using the standard χ^2 test) that about 750 events would be required to rule out the UED curve at the 99.9% c.l. Note that this number is smaller than those obtained in the previous section, indicating that the performed cuts actually enhance the difference between the MSSM and UED distributions. On the other hand, the actual discriminating power of the analysis is likely to be somewhat lower than this estimate, since the systematic uncertainty in the cut efficiencies was not taken into account here.

Our parton-level analysis does not explicitly take into account the smearing effect due to the finite jet energy and direction resolution of a real detector. The hadronic calorimeter energy resolution for a jet of energy E can be approximated by

$$\frac{\delta E}{E} \approx 0.05 + \left(\frac{1\ \mathrm{GeV}}{E}\right)^{0.5}, \tag{4.14}$$

and is in the $5-15\%$ range for the jets that pass the cuts (4.13). We can crudely estimate $\delta s/s$ to be of order $2\delta E/E$, evaluated at $E = \sqrt{s}$. The fractional uncertainty of the measurement of s in our analysis is then roughly between 10% (for points with $s \sim s^{\max}$) and 30% (for points with low s). The bin size used in figure 9 is of the order of this uncertainty for large s, and larger for small s, so we expect that the smearing introduced by binning in our analysis provides a reasonable, if crude, description of the expected smearing due to finite jet energy resolution. A more detailed investigation of this effect, and other potential detector effects, would be required to fully understand the applicability of the proposed method in a realistic experimental situation.

5. Conclusions

In this paper, we have investigated how the dijet invariant mass distributions from three-body decays of a color-octed TeV-scale new particle, such as the gluino of the MSSM and the KK gluon of the UED model, can be used to determine the nature of this particle. The production cross section for the color-octet state at the LHC is expected to be large, and the branching ratio for the three-body decays is significant whenever all squarks/KK quarks are heavier than the gluino/KK gluon. If this is the case, the dijet invariant mass distribution can be determined accurately at the LHC. The main complication of the analysis is that the distributions in the two models we considered depend on a number of parameters in addition to the spin of the decaying particle. However, even allowing for complete ignorance of these parameters, we found the dijet invariant mass to be a very promising tool for model discrimination.

The simplified analysis of this paper did not take into account a number of potentially important effects. Since the particles involved are colored, the QCD loop corrections to the

decay amplitudes are expected to be significant, and may modify the tree-level distributions we studied. Also, our analysis is performed at the parton level and does not include detector effects. While we expect that many systematic effects would cancel out since the analysis relies only on the shapes of the distributions and is insensitive to the overall normalization, a better understanding of the systematics is required. We believe that the promising conclusions of this preliminary analysis motivate a more detailed study of these issues.

Acknowledgments

We are grateful to Matt Reece and Itay Yavin for useful discussions. This research is supported by the NSF grant PHY-0355005. C.C. is also supported in part by the DOE OJI grant DE-FG02-01ER41206.

A. Polarization analysis of the UED case

The main feature of the invariant mass distribution of the UED case, which makes it distingishable from SUSY, is the dip at $s = 0$. This feature can be understood by analyzing the decay amplitudes of the individual polarization components of the mother and daughter particles and considering conservation of angular momentum. As shown with the two toy models in section 3, conservation of angular momentum can lead to suppression of the invariant mass distributions with respect to the pure phase space distribution (2.8) at $s = 0$, as well as at $s = s^{\max}$. The couplings in the UED case have the same chiral structure as the second toy model of section 3, with the quark and antiquark having opposite helicities. The added complication in the UED case is that the mother and daughter particles are massive spin one particles. We use $m_z(A)$ and $m_z(B)$ to denote the projections of the A and B spins on the direction of the momentum p_1 of the quark q. These operators have eigenvalues $m_z(A), m_z(B) = -1, 0, +1$; the corresponding eigenstates have polarization vectors ϵ_-, ϵ_L, and ϵ_+. The transitions among these eigestates are described by a 3×3 matrix of decay amplitudes. Using the UED lagrangian (4.6), we have evaluated these amplitudes and obtained the dijet invariant mass distribution corresponding to each entry.[3] These distributions, divided out by the pure phase space distribution (2.8), are plotted in figure 10. At $s = 0$ the spin projections of the quark-antiquark pair sums up to zero, and the final state has no angular momentum (see the right panel of figure 2). Therefore the polarizations of A and B must be the same. This will result in a suppression of all non-diagonal components in the transition matrix at $s = 0$, resulting in a dip there. At $s = s^{\max}$, however, the spin projections of the quark-antiquark pair add up to $m_z = +1$ (see figure 2). Thus the only allowed decays at $s_{\max}$ are the longitudinal component of A to $m_z(B) = -1$ and $m_z(A) = +1$ to the longitudinal component of B. Both features at the ends of the distribution can be nicely observed in figure 10.

[3]For clarity, we only included the contribution of the diagrams with Q_L^1 in the intermediate state. The diagrams with Q_R^1 lead to distributions that are identical, up to a parity reflection, to the ones presented here.

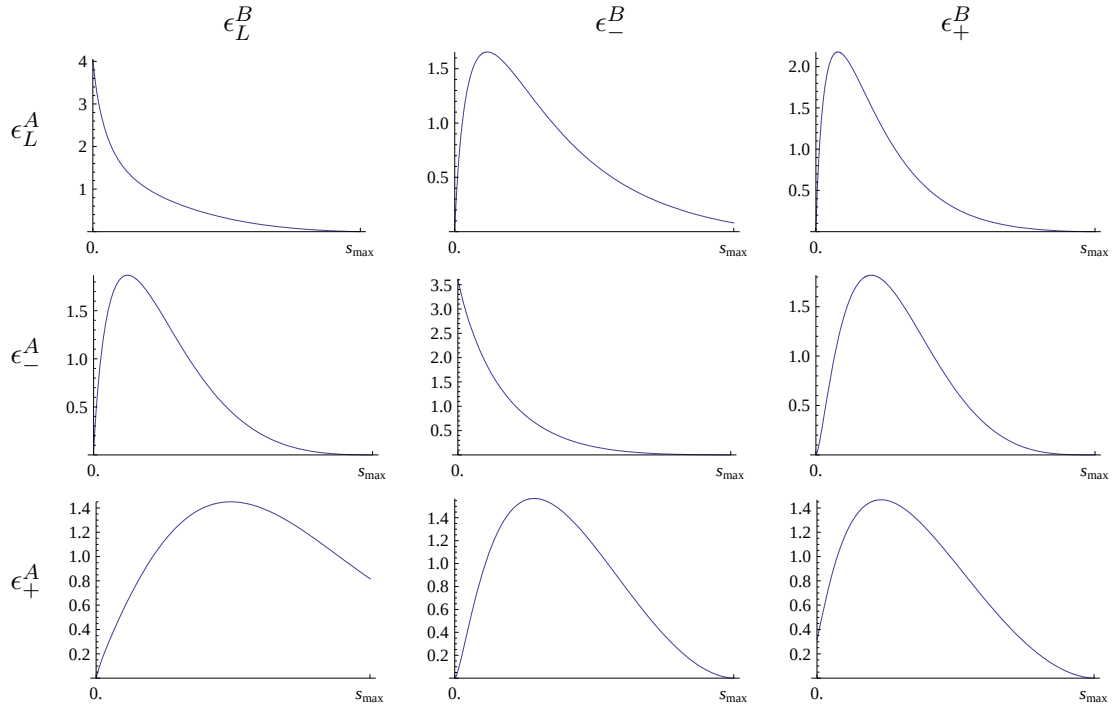

Figure 10: The invariant mass distributions for the decay of individual polarizations, divided by the phase space distribution, for $m_B/m_A = 0.1$ and $M/m_A = 1.5$ in arbitrary units. The polarization vectors are along the momentum p_1 of the outgoing quark q. Notice that at $s = m_{12}^2 = 0$ only the diagonal elements are unsuppressed due to angular momentum conservation, resulting in a dip of the distribution.

B. The Kullback-Leibler distance

A convenient measure to quantify how much two continuous probability distributions differ from each other is the *Kullback-Leibler distance*. (For a recent application in the collider phenomenology context, see ref. [4].) In this appendix, we will briefly review this measure.

Suppose that the data sample consists of N events distributed according to the theoretical prediction of model T. Consider a second model, S, which predicts a distribution different from T. We can quantify the discriminating power of our data sample by the ratio of conditional probabilities for S and T to be true, given the data:

$$\kappa = \frac{p(S \text{ is true}|N \text{ events from } T)}{p(T \text{ is true}|N \text{ events from } T)}. \tag{B.1}$$

This equation can be rewritten using Bayes' theorem:

$$\begin{aligned} \kappa &= \frac{p(S|N \text{ events from } T)}{p(T|N \text{ events from } T)} \\ &= \frac{p(S)p(N \text{ events from } T|S)}{p(T)p(N \text{ events from } T|T)} \end{aligned} \tag{B.2}$$

where $p(S)$ and $p(T)$ are the priors — probabilities for S and T to be true before the experiment at hand is conducted. (In this paper, we assumed that the MSSM and UED are

a priori equally likely, so we set $p(S) = p(T) = 1$.) Suppose that each event i ($i = 1 \ldots N$) is characterized by a single variable s_i (in our case, the dijet invariant mass). Since the N events are independent, we have

$$\begin{aligned}\kappa &= \frac{p(S)}{p(T)} \frac{\prod_{i=1}^{N} p(s_i^{(T)}|S)}{\prod_{i=1}^{N} p(s_i^{(T)}|T)} \\ &= \frac{p(S)}{p(T)} \exp\left(\sum_{i=1}^{N} \log\left(\frac{p(s_i^{(T)}|S)}{p(s_i^{(T)}|T)}\right)\right).\end{aligned} \tag{B.3}$$

For large N we can approximate $\sum_N \approx \int ds \frac{dN}{ds}$ and use the normalization condition $\frac{dN}{ds} = N p(s|T)$ to obtain

$$\begin{aligned}\kappa &\approx \frac{p(S)}{p(T)} \exp\left(N \int ds \log\left(\frac{p(s|S)}{p(s|T)}\right) p(s|T)\right) \\ &= \frac{p(S)}{p(T)} \exp\left(-N \, \mathrm{KL}(T,S)\right),\end{aligned} \tag{B.4}$$

where the *Kullback-Leibler distance* (also called *relative entropy*) is defined as

$$\mathrm{KL}(T,S) := \int ds \log\left(\frac{p(s|T)}{p(s|S)}\right) p(s|T). \tag{B.5}$$

It follows that the number of events needed to constrain the probability of model S being true, relative to the probability of T being true, to be less than $1/R$, is given by

$$N \approx \frac{\log R + \log \frac{p(S)}{p(T)}}{\mathrm{KL}(T,S)}. \tag{B.6}$$

This number provides a convenient and physically meaningful measure of how different the S and T distributions are.

Two properties of the Kullback-Leibler distance are worth mentioning in our context. First, while this is not manifest from its definition, the KL distance is non-negative, and zero if and only if $T = S$. Second, it is invariant under transformations $s \to f(s)$: for example, it does not matter whether we consider the jet invariant mass distribution in terms of s or $m_{jj} = \sqrt{s}$.

References

[1] A.J. Barr, *Using lepton charge asymmetry to investigate the spin of supersymmetric particles at the LHC*, *Phys. Lett.* **B 596** (2004) 205 [hep-ph/0405052].

[2] J.M. Smillie and B.R. Webber, *Distinguishing spins in supersymmetric and universal extra dimension models at the Large Hadron Collider*, *JHEP* **10** (2005) 069 [hep-ph/0507170].

[3] A. Datta, K. Kong and K.T. Matchev, *Discrimination of supersymmetry and universal extra dimensions at hadron colliders*, *Phys. Rev.* **D 72** (2005) 096006 [*Erratum ibid.* **D 72** (2005) 119901] [hep-ph/0509246].

JHEP10(2007)107

[4] C. Athanasiou, C.G. Lester, J.M. Smillie and B.R. Webber, *Distinguishing spins in decay chains at the large hadron collider*, *JHEP* **08** (2006) 055 [hep-ph/0605286].

[5] L.-T. Wang and I. Yavin, *Spin measurements in cascade decays at the LHC*, *JHEP* **04** (2007) 032 [hep-ph/0605296].

[6] C. Kilic, L.-T. Wang and I. Yavin, *On the existence of angular correlations in decays with heavy matter partners*, *JHEP* **05** (2007) 052 [hep-ph/0703085].

[7] A. Alves, O. Eboli and T. Plehn, *It's a gluino*, *Phys. Rev.* **D 74** (2006) 095010 [hep-ph/0605067].

[8] M. Toharia and J.D. Wells, *Gluino decays with heavier scalar superpartners*, *JHEP* **02** (2006) 015 [hep-ph/0503175].

[9] H.E. Haber and G.L. Kane, *The search for supersymmetry: probing physics beyond the standard model*, *Phys. Rept.* **117** (1985) 75.

[10] M. Perelstein and C. Spethmann, *A collider signature of the supersymmetric golden region*, *JHEP* **04** (2007) 070 [hep-ph/0702038].

[11] T. Appelquist, H.-C. Cheng and B.A. Dobrescu, *Bounds on universal extra dimensions*, *Phys. Rev.* **D 64** (2001) 035002 [hep-ph/0012100].

[12] M.S. Carena, T.M.P. Tait and C.E.M. Wagner, *Branes and orbifolds are opaque*, *Acta Phys. Polon.* **B33** (2002) 2355 [hep-ph/0207056].

[13] I. Hinchliffe, F.E. Paige, M.D. Shapiro, J. Soderqvist and W. Yao, *Precision SUSY measurements at LHC*, *Phys. Rev.* **D 55** (1997) 5520 [hep-ph/9610544].

[14] C.G. Lester and D.J. Summers, *Measuring masses of semi-invisibly decaying particles pair produced at hadron colliders*, *Phys. Lett.* **B 463** (1999) 99 [hep-ph/9906349];
A. Barr, C. Lester and P. Stephens, m_{T2}*: the truth behind the glamour*, *J. Phys.* **G 29** (2003) 2343 [hep-ph/0304226].

[15] P. Meade and M. Reece, *Top partners at the LHC: spin and mass measurement*, *Phys. Rev.* **D 74** (2006) 015010 [hep-ph/0601124].

[16] `MadGraph/MadEvent v4` can be downloaded from http://madgraph.phys.ucl.ac.be/;
For a discussions of the `Madgraph` project, see F. Maltoni and T. Stelzer, *MadEvent: automatic event generation with MadGraph*, *JHEP* **02** (2003) 027 [hep-ph/0208156];
J. Alwall et al., *MadGraph/MadEvent v4: the new web generation*, *JHEP* **09** (2007) 028 [arXiv:0706.2334].

[17] *CMS Physics TDR: V. II, Physics Peformance*, CERN-LHCC-2006-021 (2006).

JHEP10(2007)107